A Framework for Aerial Inspection of Siltation in Waterways

Hamza Anwar
Dept. of Electrical Engineering
SBA School of Science & Engineering
LUMS, Pakistan
hmza.anwr@gmail.com

Abubakr Muhammad
Dept. of Electrical Engineering
SBA School of Science & Engineering
LUMS, Pakistan
abubakr@lums.edu.pk

Karsten Berns
Robotics Research Lab
Department of Computer Science
University of Kaiserslautern, Germany
berns@cs.uni-kl.de

***Abstract*—Silt accumulation and sedimentation in canal beds leads to deterioration of watercourses over time. Every year a forced closure of the canals in the Indus basin is inevitable for canal cleaning, entailing a very large scale and costly operation. Silt removal precision is prone to inefficiencies due to subjective decision making in the cleaning process. In this paper, we lay out a theoretical framework to map the semi-structured (emptied) canal bed terrains with an Unmanned Aerial Vehicle (UAV) system for quantitative inspection of deposited silt. The study employs Gaussian process regression on sampled points to determine a continuous distribution of silt surface, thereby, predicting the volume of silt on canal bed. Our theoretical analysis builds upon certain mathematical bounds on the variance of estimated volume, while explicitly considering localization error and sensor noise. Essentially, we setup a framework for studying how tolerable are the process and measurement uncertainties, while achieving a desired accuracy in silt profile and corresponding volume. We demonstrate the regression results in simulations as well as lab-scaled-model (LMS151 laser scanner) with different sets of parameters. Volume estimation is verified practically and mathematical performance limits are proposed in established aerial canal inspection system.**

I. Introduction

Inspecting man-made structures or rough outdoor terrains for physical defects, deterioration, usability and safety, involves human inspectors to do safety-critical, expensive and time-consuming engineering tasks. Automating these, is a hot topic and has paved way for research developments in aerial, water and ground robotics [9][13][11]. Robotic platforms that can create fast, accurate and detailed 3D models with fused imagery, for inspections are in the making. All this has led to high-end reliable sensors and precise actuators. However, the need of quantitative analysis of material surfaces inspected along with a theoretical study for maximizing inspection performance, has not been exclusively addressed. Our interest in inspecting and mapping surfaces focuses on maximizing volumetric estimation accuracy of granular media in outdoor terrains for problems like canal cleaning, landscaping, mining, and excavation.

Recently, a lot of work in inspecting safety, productivity and health in infrastructures and industrial facilities has been done using aerial and marine robots. Sa et al. [20] have proposed control and perception algorithms for pole detection in high frame-rates of a pole inspection UAV system. A similar work by Burri et al. [4] is done on the implementation of a flying robot to inspect industrial plant boiler systems. They have concentrated on robust control strategies under real-time constraints for boiler inspection. Some researchers [15] have developed a Micro-Aerial Vehicle (MAV) assistance system to inspect large naval vessels. Moreover, there is work available on building flight navigation in unstructured environments [2][3]. Others have managed inspection of the environment by physical interaction of MAVs [5][8]. Most of these works address implementation schemes and not undertake analysis of accuracy limits of inferred surfaces.

The civil engineering community has also employed robotic solutions to inspect infrastructure for faults. A group from KAIST [10], has talked about an inspection robot system that attaches itself to a structure and measures the structural displacement in 6-DOF. For bridge inspection, Murphy et al. [14], have made use of Unmanned Marine Vehicles (UMV). They have also developed a UAV-UMV system for littoral environments [18][13] in military applications. Note that, a common factor in these works is the deployment aspect of such field robots. These works use robotic platforms in structural inspection attending issues of obstacle avoidance, controller design and pose estimation.

In the context of unstructured terrain mapping, we are currently not concerned with navigation. In most works related to outdoor terrains both the aspects are covered together. Due to uneven roughness, navigation and obstacle avoidance become hard problems. For rough terrains, approximating surface maps to planes has been found useful [11][21]. The task of surface estimation reduces to finding a collection of planar surfaces. Although this is an advantage when implementing such systems, such studies don't address the rich theoretical analysis that can tell the accuracy limits of estimates. Most importantly, the end objectives of mapping in such applications is acceptable navigation, and not to find the ground truth of encountered terrains. Most relevant to our current work is research by groups from Carnegie Mellon University [7] and University of Freiburg [12]. Handsell et al. [7] present a kernel-based learning approach to estimate continuous surfaces over rough terrain to employ a better control in navigation and obstacle avoidance.

This work is funded by LUMS Faculty Initiative Fund (FIF) and German Academic Exchange Service (DAAD) for the project *RoPWat*.

Fig. 1. Bank deterioration (left) and siltation (right) in irrigation canals.

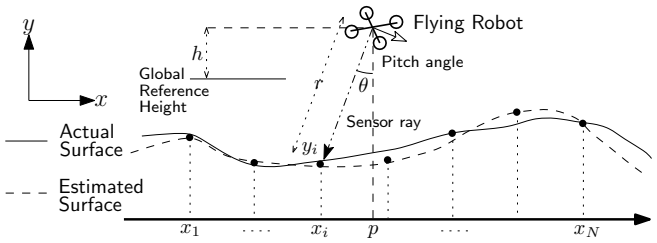

Fig. 2. Side view of a silted canal bed being profiled by a flying robot.

This prediction [7] has led to upper and lower bounds on the continuous estimated terrain surface. Lang et al. [12] use Gaussian Process regression with non-stationary kernel for accurate terrain modeling of local discontinuity. Their work is further improved and extended later [16]. The key difference in our work and the mentioned works is our explicit incorporation of probabilistic models of robot's localization and sensor noise in our framework.

The motivation for our work comes from a desire to map the large irrigation canal network in the Indus basin for studying siltation. Water supply to the agricultural base in Pakistan's Indus river basin is through a vast network of irrigation canals that run more than 50,000 km in length. Most of the canals have mud banks and beds which undergo deterioration over time due to accumulation of silt and sediment transported by the rivers. See Fig. 1 for some situations. A forced closure of the canals is inevitable for canal cleaning, yearly, entailing a large scale and costly operation. The extent and precision of silt removal is prone to inefficiencies due to subjective decision making in the process, shortage of time and lack of verification. We aim to develop a semi-autonomous robotic profiling system to increase the efficiency of this process. We propose to develop a 3D perception system, which will be deployed on board an aerial robot to assist the human operator in surveying and cleaning the canal effectively during the annual canal closures. The current manual system decides on cleaning based on measurements taken every 1000 feet. It looks for at least 6 inch silt depth at these data points. Proposed system envisages efficient cost effective cleaning, reduced water discharge variability, and enhanced agricultural productivity. While a team of roboticists in our respective groups is working on various implementation aspects of the project (algorithms, control, post-processing of acquired data), this paper aims to investigate the achievable performance limits of the proposed aerial canal inspection system in theory.

Our survey shows that there are two distinct areas relating to the problem in hand. On one side, there is work in structural inspection suited for precisely defined environments and, on the other, is work on mapping rough uneven surfaces. In our interest, canals offer a semi-structured environment which neither provides a geometric uniformity (like bridges and buildings), nor a relaxation in representation (like fields and forests). Although there's work on river exploration [9] and other similar tasks, the key point of our work is a probabilistic analysis of how inspection of accumulated silt can improve net canal cleaning performance.

In the past, we have done work on the task of volume estimation of soil by visual inspection algorithms [1]. The goal was to develop a standalone system that measures quantities of any granular material inside a container whose model we acquire separately. We developed a methodology to estimate soil quantities in a bucket excavator, using a stereo vision system. Our approach was to make dense 3D point cloud of the contained material and compare it with an empty container model. Planes were fit over the soil surface using RANdom SAmple Consensus (RANSAC) algorithm, and the difference between the two surfaces was accumulated to give total material volume. Note that, our goal in this paper is not to devise a new algorithm in place of our previous work [1], but we aim to determine theoretical bounds on our estimates for canal cleaning application. Moreover, this work incorporates sensor mobility and associated errors, while in previous work the sensor is assumed to be static.

In this paper, we have derived mathematical relationships relating the positioning and sensing uncertainty of robotic inspection vehicles with estimation of the uneven surface profiles and their corresponding enclosed volumes. We setup the canal inspection problem in a basic one-dimensional setting and discuss the sources of uncertainty in robot's localization and sensing. We then regress the scanned surface points into a Gaussian process which gives a mean silt surface surrounded by a confidence interval. Volume encapsulated by this surface is determined by comparing it with previously scanned surface. The mean surface and the confidence interval lead to expressions of scalar mean volume and its variance. An analysis of these expressions that shows how tolerable are the localization and sensor uncertainties, for achieving desired accuracy in profiling and corresponding volume estimate. In the end, synthetic lab-scaled experimentation to verify feasibility is presented, whose accurate results strengthen our position in deploying our proposed framework on real large-scale grounds.

II. Problem Setup

Consider a canal that has accumulated silt on its surface, and a flying robot is moving along the dried channel, scanning it from above (See Fig. 2). We assume that the canal is dried up and their is no pooling of water with the silted canal bed completely exposed. We've simplified the scanning problem to a single dimension. The major argument for it being the canal structure which is similar to that of a road. So, we can't measure depth along the channel length by taking scans from single point in space, on the contrary, the width of canal is such that the 3D sensor can scan across it in a single scan, see cross-sectional canal view in Fig. 3. Robot is moving along the canal and since surface fitting is independent along orthogonal axes, so the

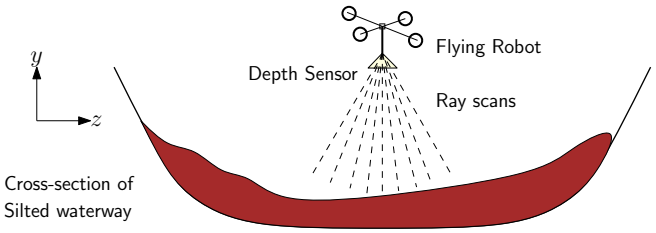

Fig. 3. Cross-sectional view of a silted canal bed profiled by a flying robot.

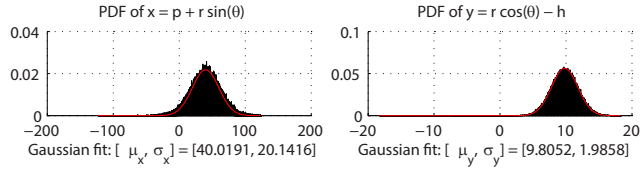

Fig. 4. Black bars show actual density functions of x and y, where $[\hat{p}, \sigma_p^2, \hat{h}, \sigma_h^2, \hat{r}, \sigma_r^2, \hat{\theta}, \sigma_\theta^2, N] = [40, 20, 0, 0.1, 10, 2, 0, 0.2, 2 \times 10^5]$.

problem reduces to single dimension. In principle, the methods discussed in this paper can be generalized to profile full 2D canal surface to assess bank deterioration. The mounted sensor, owing to robot's localization error, has uncertain position and orientation throughout the operation. Secondly, the sensor also exhibits a noise in its measurements.

The robot's pose vector, $\mathbf{x} = [p \ h \ \theta]^\top$, consists of its position along canal's axis, it's height from global reference height and angle tilt in the sensor facing downward. All three variables are independent and distributed normally, and likewise, the range sensor returns are also normally distributed. The 2D point on silt surface scanned for each measurement is (x, y). So, we have the following relations,

$$p \sim \mathcal{N}(\hat{p}, \sigma_p^2), \ \ h \sim \mathcal{N}(0, \sigma_h^2), \ \ \theta \sim \mathcal{N}(0, \sigma_\theta^2), \ \ r \sim \mathcal{N}(\hat{r}, \sigma_r^2).$$

$$x = p + r\sin\theta, \qquad y = r\cos\theta - h.$$

The distribution for the random variables x and y can be approximated by a gaussian because of its similar density function shape, as shown in Fig. 4. Hence, we can algorithmically, identify the exact values of variances in x and y. However, for this paper, we will approximate $\sigma_x^2 \approx \sigma_p^2$ and $\sigma_y^2 \approx \sigma_r^2$. A practical choice of parameters verifies such an approximation, see Fig. 4 ($20.141 \approx 20$ and $1.985 \approx 0.2$).

$$x \sim \mathcal{N}(\hat{p}, \sigma_x^2) \approx \mathcal{N}(\hat{p}, \sigma_p^2) \qquad y \sim \mathcal{N}(\hat{r}, \sigma_y^2) \approx \mathcal{N}(\hat{r}, \sigma_r^2).$$

A. Estimating the silt surface

With these sources of uncertainty, an algorithm measures the volume of the silt accumulated on the canal bed. Our goal is to determine theoretical limits on the achievable accuracy when estimating silt volume. But first a surface representation, $f(x)$, from scanned points $\{(x_i, y_i)\}_{i=1}^N$, $y_* = f(x_*)$ is needed. A nice representation must have nearby points that are correlated. Beyond a certain resolution details of the surface become unnecessary. Set of scanned points act as landmarks to fit a regression model which gives a surface enforcing stronger correlation between nearby and weaker between faraway points, respecting smoothness and handling ease. Our choice of a good candidate for such representation is a Gaussian process, $f(x)$, which is defined by a mean ($\mu(x)$) and covariance functions ($k(x_i, x_j)$).

B. Estimating volume of silt

In determining mean silt volume and corresponding variance, an expression for integrating the gaussian random process is required. Recall that the mean-square integral of a random process $f(x)$ over the interval $[-W, W]$ is a random variable, Y_X, defined as the limiting sum given by,

$$Y_X = \int_{-W}^{W} f(x)dx = \lim_{n\to\infty \Delta_k \to 0} \sum_{k=0}^{n-1} f(x_k)\Delta_k.$$

A sufficient condition for mean-square integral, Y_X to exist is that the double integral, $\int_{-W}^{W}\int_{-W}^{W} \mathcal{R}_f(x_1, x_2)dx_1dx_2$, exists. For our case Σ_f, the covariance matrix, exists and it directly relates to $\mathcal{R}_f$, the autocorrelation function, which implies that Y_X will exist. Denote area under the silt's surface as $A = Y_X$. From now on, we will use the terms area and volume interchangeably. We will consider the silt to be defined within $[-W, W]$ which basically are ends of the canal in robot's view. Determining area's mean μ_A and variance σ_A^2:

$$\mu_A = \mathrm{E}[\int f(x)dx] = \int \mathrm{E}[f(x)]dx = \int_{-W}^{W} \mu_f dx,$$

$$\sigma_A^2 = \mathrm{E}[Y_{X_1} Y_{X_2}] = \int_{-W}^{W}\int_{-W}^{W} \Sigma_f(x_1, x_2)dx_1dx_2.$$

III. GP Regression: Estimating $f(x)$

This section will work out expressions for different cases of localization error and sensor noise. Its contents are extracted from Girard [6] and Rasmussen et al. [19].

A. No localization error

1) No sensor noise: Let's start with the completely noise-free base case that'd be built upon. For covariance function, we chose the squared exponential kernel function due to its wide usage, differentiability and smoothness. Moreover, this kernel can theoretically give exact solutions even in noisy case. In determining the distribution $p(f(x)|x, x_*, y_*)$ where $(x_*, y_*) \in \{(x_i, y_i)\}_{i=1}^N$, since y_* and $f(x)$ are Gaussian, we'd have a joint Gaussian distribution of y_* and $f(x)$.

$$k(x_p, x_q) = ve^{-(x_p - x_q)^2/(2w)}.$$

$$\begin{bmatrix} y_* \\ f(x) \end{bmatrix} \sim \mathcal{N}\Big(0, \begin{bmatrix} K(x_*, x_*) & K(x_*, x) \\ K(x, x_*) & K(x, x) \end{bmatrix}\Big),$$

where, $K(x_*, x_*)$ is an $N \times N$ matrix defining covariance of the training samples; $K(x, x)$ denotes covariance matrix of all test points; and other two terms are for cross-covariances. $\mathbf{y}_*$ is N dimensional vector of scanned points; $\mathbf{k}_* := K(x, x_*) = K(x_*, x)^\top$, $K_{xx} := K(x, x)$ and $K := K(x_*, x_*)$. By marginalizing over y_* we get:

$$p(f(x)|x, x_*, y_*) \sim \mathcal{N}\Big(K(x, x_*)(K(x_*, x_*))^{-1}\mathbf{y}_*, \\ K(x, x) - K(x, x_*)(K(x_*, x_*))^{-1}K(x_*, x)\Big),$$

$$\Rightarrow \ p(f(x)|x, x_*, y_*) \sim \mathcal{N}(\mathbf{k}_*^\top K^{-1}\mathbf{y}_*, K_{xx} - \mathbf{k}_*^\top K^{-1}\mathbf{k}_*).$$

$$\Rightarrow \quad \mu_f = \mathbf{k}_*^\top K^{-1}\mathbf{y}_*, \qquad \Sigma_f = K_{xx} - \mathbf{k}_*^\top K^{-1}\mathbf{k}_*,$$

2) With sensor noise: For a non-zero sensor noise, our scanned points $\mathbf{y}_*$ now have uncertainty. Since we are assuming sensor noise to be uncorrelated between samples so it's effect appears only along the diagonal of K, i.e.

$$\mu_f = \mathbf{k}_*^\top (K + \sigma_r^2 \mathbf{I})^{-1} \mathbf{y}_*,\ \Sigma_f = K_{xx} - \mathbf{k}_*^\top (K + \sigma_r^2 \mathbf{I})^{-1} \mathbf{k}_*.$$

B. With localization error

For the full noisy case, expressions becomes complicated. Here, our training data has localization error i.e. $x_i \sim \mathcal{N}(\hat{p}_i, \sigma_{p_i}^2)$. We see that kernel function alters because of variance in x_i. Taking constant mean prior on $f(x)$ i.e. $\text{Var}[\text{E}_x[y_i|x_i]] = 0$, and by law of iterated expectation:

$$\text{Var}[y_i|\hat{p}_i] = \text{E}_x[\text{Var}[y_i|x_i]] + \text{Var}[\text{E}_x[y_i|x_i]],$$
$$\text{Cov}[y_i, y_j|\hat{p}_i, \hat{p}_j] = \iint \text{Cov}[y_i, y_j|x_i, x_j] p(x_i, x_j) dx_i dx_j.$$

Assuming that any two random points on the ground from the training data, are independent random variables (i.e. $p(x_i, x_j) = p(x_i)p(x_j)$) and that all have the same variance term, $\sigma_{p_i}^2 = \sigma_{p_j}^2 = \sigma_p^2$. Recall that kernel function, $k(x_i, x_j) = \text{Cov}[y_i, y_j|x_i, x_j] = ve^{-(x_i - x_j)^2/(2w)}$, is squared-exponential, and x as well, is distributed normally,

$$k_{\text{noisy}}(\hat{p}_i, \hat{p}_j) = \iint \mathcal{N}(0, w)\mathcal{N}(\hat{p}_i, \sigma_p^2)\mathcal{N}(\hat{p}_j, \sigma_p^2) dx_i dx_j.$$

$$\Rightarrow k_{\text{noisy}}(\hat{p}_i, \hat{p}_j) = v' e^{-(\hat{p}_i - \hat{p}_j)^2/(2w')}. \tag{1}$$

where, $v' = v(1 + 2w\sigma_p^2)^{-1/2}$ and $w' = w + 2\sigma_p^2$. This step is achieved by reducing the product of Gaussians and integrating over all x_i and x_j. Now, in the end we see that the effect of localization error is a change in the horizontal and vertical length-scales of the covariance function of our Gaussian process, while preserving the shape. We have similar expressions of μ_f and Σ_f with noisy kernel function:

$$\mu_f = \mathbf{k}_{*,\text{noisy}}^\top (K_{\text{noisy}} + \sigma_r^2 \mathbf{I})^{-1} \mathbf{y}_*,$$
$$\Sigma_f = K_{xx,\text{noisy}} - \mathbf{k}_{*,\text{noisy}}^\top (K_{\text{noisy}} + \sigma_r^2 \mathbf{I})^{-1} \mathbf{k}_{*,\text{noisy}}.$$

C. Optimal hyperparameter selection

For optimal length scales (kernel parameters) combination, we need to maximize this log marginal likelihood. Among various methods, we used grid-based search to best fit our acquired data, giving $v = 6.15$ and $w = 4.65$.

$$\log p(\mathbf{y}_*|\mathbf{x}_*, v, w) = -\tfrac{1}{2}\mathbf{y}_*(K + \sigma_r^2 \mathbf{I})^{-1}\mathbf{y}_* - \tfrac{1}{2}\log|K + \sigma_r^2 \mathbf{I}| - \tfrac{n}{2}\log 2\pi$$

IV. Theoretical bounds on the variance of volume estimate (σ_A^2)

In this section we establish certain bounds on σ_A^2 in terms of σ_p^2, σ_r^2 and the process parameters (w and v). Remember,

$$\Sigma_f(t, s) = K_{xx}(t, s) - \mathbf{k}_*^\top(t, s)[K + \sigma_r^2 \mathbf{I}]^{-1} \mathbf{k}_*(t, s), \tag{2}$$

$$\sigma_A^2 = \int_{-W}^{W}\int_{-W}^{W} \Sigma_f(t, s) dt ds. \tag{3}$$

For ease in comparison, we will index the training samples, x_*, as x_i.

We solve this integral in two parts. The term $K_{xx}(t, s)$ in (2) has a simple form defined by $k_{\text{noisy}}(t, s)$ in (1),

$$\iint K_{xx}(t, s) dt ds = \iint v' e^{-(t-s)^2/(2w')} dt ds,$$
$$= 2v'\Big(w' e^{-2W^2/w'} - w' + W\sqrt{2\pi w'}\,\text{erf}(W\sqrt{\frac{2}{w'}})\Big), \tag{4}$$

where $\text{erf}(x) = \frac{2}{\sqrt{\pi}}\int_0^x e^{-t^2} dt$. For integrating the second term in (2) define,

$$H(t, s) := \mathbf{k}_*^\top(t, s)[K + \sigma_r^2 \mathbf{I}]^{-1} \mathbf{k}_*(t, s).$$

Because of the matrix inversion in the quadratic form, we simplify by truncating, and thus solve keeping in mind that the expression is strictly positive definite:

$$H_0(t, s) := \mathbf{k}_*^\top(t, s)[\sigma_r^2 \mathbf{I}]^{-1} \mathbf{k}_*(t, s),$$
$$\iint H_0(t, s) dt ds = \iint \sum_{i=1}^{n} \frac{k(a, i)k(b, i)}{\sigma_r^2} dt ds,$$
$$= \frac{v'^2}{\sigma_r^2}\sum_{i=1}^{n}\iint e^{-((t-x_i)^2 + (s-x_i)^2)/(2w')} dt ds,$$
$$= \frac{\pi w' v'^2}{2\sigma_r^2}\sum_{i=1}^{n}[\text{erf}\Big(\frac{x_i - W}{\sqrt{2w'}}\Big) - \text{erf}\Big(\frac{x_i + W}{\sqrt{2w'}}\Big)]^2 \leqslant \frac{\pi w' v'^2}{2\sigma_r^2} 4n. \tag{5}$$

The fact that $-1 \leqslant \text{erf}(x) \leqslant 1\ \forall\ x \in \mathbb{R}$ has lead us to the above inequality. To relate the two, we highlight certain key points while avoiding singularities in inversion,

- Sensors are never perfect, i.e. $\sigma_r^2 > 0$.
- Note that, $\mathbf{k}_*(t, s) \geqslant 0\ \forall\ (t, s) \in \mathbb{R}^2$. This pops from the use of squared exponential kernel (1).
- The covariance matrix of training data, K, is positive definite, i.e. $K \succ 0$, with all individual entries being positive real numbers (choice of kernel).

With these points, we can safely argue that,

$$\mathbf{k}_*^\top (K + \sigma_r^2 \mathbf{I})^{-1} \mathbf{k}_* \preceq \mathbf{k}_*^\top (\sigma_r^2 \mathbf{I})^{-1} \mathbf{k}_*,$$
$$\iint \mathbf{k}_*^\top [K + \sigma_r^2 \mathbf{I}]^{-1} \mathbf{k}_* dt ds \leqslant \iint \mathbf{k}_*^\top [\sigma_r^2 \mathbf{I}]^{-1} \mathbf{k}_* dt ds,$$
$$\Rightarrow \iint H(t, s) dt ds \leqslant \iint H_0(t, s) dt ds. \tag{6}$$

From (2), (3), (6), and the definitions of $H(t, s)$ and $H_0(t, s)$, we construct the inequality,

$$\sigma_A^2 \geqslant \int_{-W}^{W}\int_{-W}^{W} K_{xx}(t, s) dt ds - \int_{-W}^{W}\int_{-W}^{W} H_0(t, s) dt ds.$$

Thus, incorporating (4) and (5), we arrive at a lower bound on the volume variance,

$$\sigma_A^2 \geqslant 2v'w'\Big(e^{\frac{-2W^2}{w'}} - 1 - \frac{n\pi v'}{\sigma_r^2} + W\sqrt{\frac{2\pi}{w'}}\,\text{erf}(W\sqrt{\frac{2}{w'}})\Big). \tag{7}$$

Keep in mind that the inequality due to $\text{erf}(x)$ in (5) itself is a measure of dispersion information of the training samples. So, in future, we can look for a tighter as well as a lower bound on the $\text{erf}(x)$ expression if we have knowledge about the distribution of samples.

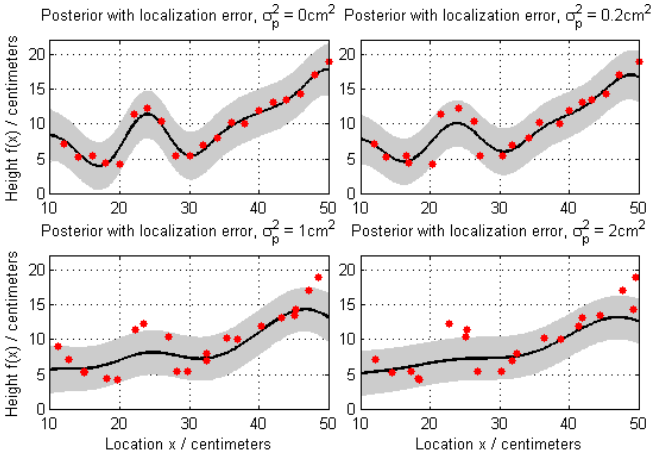

Fig. 5. Regression posterior with changing $\sigma_p^2 = [0, 0.2, 1, 2]$ cm^2. Effect of increasing position error of data points (red) along x-axis is visible. Gray region is 96% confidence tube and black curve is the mean.

V. Simulation Results

We simulated GP regression technique on custom dataset. ROI in robot's view was taken -3.5 to 3.5 meters along canal's length i.e. x-axis ($[-W, W]$). Parameters of interest include sensor resolution along robot's position axis, sensor noise in scanned points (σ_r^2), initial guess of the length scales (GP parameters – w and v) and most importantly localization error, σ_p^2. Depending on initial choice of the GP parameters (i.e. w and v, recall the kernel function from (1)), it becomes evident that w controls the smoothness of the estimate, whereas v controls deviation from mean. Likewise, the sensor noise, σ_r^2, effects the thickness of the confidence tube. An interesting series of experiments performed when we incorporated the localization error in measurements is shown in Fig. 5. Here, we corrupted our data points in both perpendicular axes (sensor noise and localization error) with corresponding normal distributions. For realistic demonstration, we also altered our initial choice of the GP parameters based on their relationships with the variance in localization estimate ($w' = w + 2\sigma_p^2$ and $v' = v(1 + 2w\sigma_p^2)^{-1/2}$). Our simulations, aimed at initial testing, gave us the green signal to conduct various experimentation (surface and volume) on scaled lab model data.

VI. Experiments on a Scaled Lab Model

A. Surface estimation experiments

Laboratory setting consisted of a bucket of 4 by 2 sq-ft wide mouth filled up with soil (Fig. 6). Sick laser scanner (LMS151) was attached with a prismatic joint to move horizontally at a height above the surface. Progressive scans of the surface were taken by periodically moving the scanner. Exact sensor position was noted using an electric potentiometer and a flat ruler. Four experiments with different profiles types each, were conducted (Fig. 7). Scanning resolution used was 2cm. Since, the scans gave cross-sectional view (similar to Fig. 3), we took the central (vertically downward) points. We assumed zero localization error because of precise 2cm movements, and sensor noise variance of 1.44cm^2 – derived from a study of LMS151 [17]. Reconstructed profiles are shown in Fig. 8.

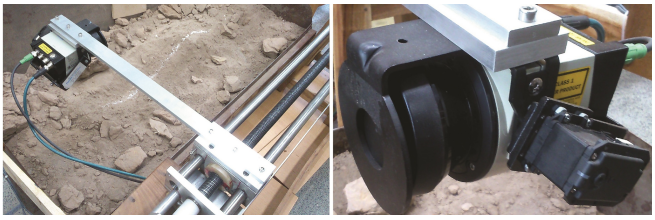

Fig. 6. Hardware assembly of scaled lab model with scanner maneuvering above along canal length axis (left). Close-up of LMS151 scanner (right).

Fig. 7. Profiles A, B, C, D (top, right, bottom, left) for surface estimation.

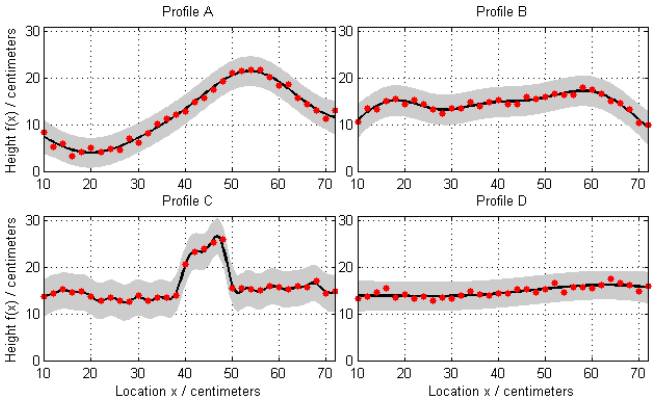

Fig. 8. GP Regression results with optimal parameters of the corresponding profiles (See Fig. 7). Note that, we took $\sigma_r^2 = 1.44$cm^2 and $\sigma_p^2 = 0$.

B. Volume experiment

For volume estimation, dig-shaped profile of the soil in our test bed was scanned, Fig. 9(a). Later, a cylindrical-shaped object with 6.6cm diameter was placed inside the dig with its length axis perpendicular to the sensor's motion and scanned again, Fig. 9(b). Optimal parameters for both states were chosen independently, and after regression corresponding profiles were plotted in Fig. 10. For volume, we overlaid the two profiles, specified ROI (i.e. where cylinder object was placed) to avoid error accumulation and measured the area of enclosed region, Fig. 11. The choice of object being cylindrical was to avoid unnecessary surface irregularities. Actual cross-sectional area of the cylinder was $\pi r^2 = 34.22$cm^2. Estimate given by numerical integration was 40.71cm^2. Volume estimate standard deviation came out to be 6.423cm^2. High deviation is due to high sensor noise (1.44cm^2) and large sampling resolution (2cm).

Fig. 9. Two states of the channel model: (a) Baseline (left); (b) Silted (right).

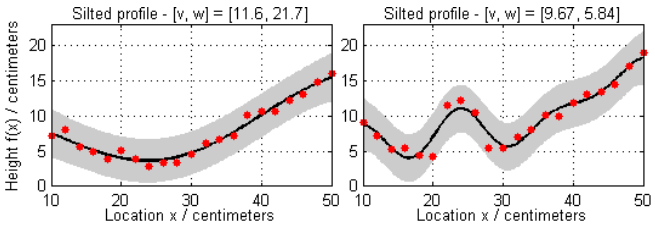

Fig. 10. Optimally estimated surfaces of Baseline (left) and Silted (right) states of channel model (See Fig.9). For both, $\sigma_r^2 = 1.44\text{cm}^2$ and $\sigma_p^2 = 0\text{cm}^2$.

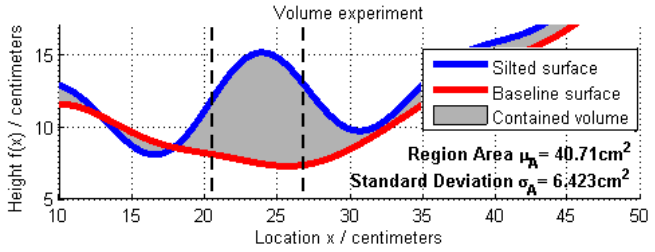

Fig. 11. Plots depicting one-dimensional view of the silt volume estimation experiment. The hump enclosed by the dashed lines represents the approximated surface of the cylindrical object used (See Fig. 9). The difference in surfaces outside this region is because of noise in sensor readings.

VII. Conclusions and Discussion

This paper is a first attempt towards analyzing accuracy of the volume estimates using probabilistic modeling of silt surfaces in canals. We use Gaussian process regression to model surfaces, considering uncertainty of robot's localization and its sensor precision. Novelty of our presented work lies in incorporation of localization error and then, arriving at closed-form expressions that limit the achievable accuracy in estimates of silt volume. Through simulations, we have seen that increased localization error effect surface estimation and corresponding volume quite significantly. The sensor noise does not disrupt the shape, rather it narrows or tightens the confidence of the estimate. We have analyzed that, for accurate inspection task, localization capability weighs more in importance over sensor accuracy. Scaled lab experiments depict feasibility and deployability of our algorithm.

In future, information of dispersion of data points and sensor resolution can help in getting tighter theoretical bounds. Full 3D sensor model and other kernel functions can also be studied. Usefulness of our work shall become apparent upon comparison of manual canal surveying process with our aerial inspection system. Note that, Gaussian process regression for large 3D point clouds is not practically efficient. However, our analysis provides useful insights before implementing any practical algorithm that looks to achieve the theoretical performance promised by an optimal estimation framework.

References

[1] H. Anwar, S. M. Abbas, A. Muhammad, and K. Berns, "Volumetric Estimation of Contained Soil using 3D Sensors," in *Intl. Commercial Vehicle Technology Symposium*, 2014, pp. 11–13.

[2] A. Bachrach, R. He, and N. Roy, "Autonomous flight in unknown indoor environments," *Intl. Jour. of Micro Air Vehicles*, vol. 1, no. 4, 2009.

[3] M. Blosch, S. Weiss, D. Scaramuzza, and R. Siegwart, "Vision based MAV navigation in unknown and unstructured environments," in *Intl. Conf. on Robotics and Automation (ICRA)*. IEEE, 2010, pp. 21–28.

[4] M. Burri, J. Nikolic, C. Hurzeler, G. Caprari, and R. Siegwart, "Aerial service robots for visual inspection of thermal power plant boiler systems," in *IEEE Applied Robotics for Power Industry (CARPI)*, 2012.

[5] G. Darivianakis, K. Alexis, M. Burri, and R. Y. Siegwart, "Hybrid Predictive Control for Aerial Robotic Physical Interaction towards Inspection Operations," in *IEEE Robotics Automation (ICRA)*, 2014.

[6] A. Girard, "Approximate methods for propagation of uncertainty with Gaussian process models," Ph.D. dissertation, Univ. of Glasgow, 2004.

[7] R. Hadsell, J. A. Bagnell, D. F. Huber, and M. Hebert, "Accurate rough terrain estimation with space-carving kernels," in *Robotics: Science and Systems*, 2009.

[8] C. Hürzeler, "Modeling and design of unmanned rotorcraft systems for contact based inspection," Ph.D. dissertation, ETH Zurich, 2013.

[9] S. Jain, S. Nuske, A. Chambers, L. Yoder, H. Cover, L. Chamberlain, S. Scherer, and S. Singh, "Autonomous River Exploration," in *Proc. of Intl. Conf. on Field and Service Robots (FSR)*, vol. 5, 2013.

[10] H. Jeon, Y. Bang, and H. Myung, "Structural inspection robot for displacement measurement," in *Intl. Conf. on Digital Ecosystems and Technologies (DEST)*. IEEE, 2011, pp. 188–191.

[11] K. Konolige, M. Agrawal, R. C. Bolles, C. Cowan, M. Fischler, and B. Gerkey, "Outdoor mapping and navigation using stereo vision," in *Experimental Robotics*. Springer, 2008, pp. 179–190.

[12] T. Lang, C. Plagemann, and W. Burgard, "Adaptive Non-Stationary Kernel Regression for Terrain Modeling." in *Robotics: Science and Systems*, 2007.

[13] M. Lindemuth, R. Murphy, E. Steimle, W. Armitage, K. Dreger, T. Elliot, M. Hall, D. Kalyadin, J. Kramer, M. Palankar *et al.*, "Sea robot-assisted inspection," *Robotics & Automation Magazine, IEEE*, vol. 18, no. 2, pp. 96–107, 2011.

[14] R. R. Murphy, E. Steimle, M. Hall, M. Lindemuth, D. Trejo, S. Hurlebaus, Z. Medina-Cetina, and D. Slocum, "Robot-assisted bridge inspection," *Jour. of Intelligent & Robotic Systems*, vol. 64, no. 1, 2011.

[15] A. Ortiz, F. Bonnin-Pascual, and E. Garcia-Fidalgo, "Vessel Inspection: A Micro-Aerial Vehicle-based Approach," *Jour. of Intelligent & Robotic Systems*, pp. 1–17, 2013.

[16] C. Plagemann, K. Kersting, and W. Burgard, "Nonstationary Gaussian process regression using point estimates of local smoothness," in *Machine learning and knowledge discovery in databases*, 2008.

[17] F. Pomerleau, A. Breitenmoser, M. Liu, F. Colas, and R. Siegwart, "Noise characterization of depth sensors for surface inspections," in *IEEE Applied Robotics for Power Industry (CARPI)*, 2012, pp. 16–21.

[18] K. S. Pratt, R. Murphy, S. Stover, and C. Griffin, "CONOPS and autonomy recommendations for VTOL small unmanned aerial system based on Hurricane Katrina operations," *Journal of Field Robotics*, vol. 26, no. 8, pp. 636–650, 2009.

[19] C. E. Rasmussen and C. K. I. Williams, *Gaussian processes for machine learning*. MIT Press, 2006.

[20] I. Sa, S. Hrabar, and P. Corke, "Outdoor flight testing of a pole inspection UAV incorporating high-speed vision," *Springer Tracts in Advanced Robotics*, 2014.

[21] H. Schäfer, M. Proetzsch, and K. Berns, "Stereo-vision-based obstacle avoidance in rough outdoor terrain," in *Intl. Symposium on Motor Control and Robotics*, 2005.